ELSEVIER

Drying–wetting approach for 3D finite element sigma coordinate model for estuaries with large tidal flats

Y.W. Jiang [a,b], Onyx W.H. Wai [a,*]

[a] *Department of Civil and Structural Engineering, The Hong Kong Polytechnic University, Hong Kong*
[b] *Key Laboratory of Marine Environmental Science, Xiamen University, Ministry of Education, 361005, China*

Abstract

An approach to represent drying and wetting processes in a three-dimensional finite element sigma coordinate model is described. This approach makes use of capillaries in dry areas, which can connect to the nearby wet areas. The time marching of the mass conservation equation is modified by introducing a "size factor" coefficient and a water level diffusion term. Therefore, the fictitious water level of the dry nodes can fluctuate with the adjacent wet nodes. This eliminates the artificial pressure gradient appearing in some drying and wetting approaches in the partially wet (transition) elements. This approach results in a null momentum computation at the dry areas, which can guarantee numerical stability and satisfy the mass and momentum conservation. The approach has been applied in a hypothetical case and a real case in Xiamen Estuary, China, with satisfactory results.
© 2005 Elsevier Ltd. All rights reserved.

Keywords: Drying and wetting; Finite element; Three-dimension; Sigma coordinate; Estuary

1. Introduction

Most of the tidal flats in estuaries are wetland. Wetland plays a very important role in the ecosystem and its productivity is maintained mainly by the periodic drying and wetting processes. At the same time, salt water and freshwater mixing is mostly a three-dimensional (3D) phenomenon. So it is necessary for an estuary numerical model to have a practical approach that not only can simulate drying and wetting processes accurately, but also can maintain stability to carry long-term 3D studies. Reviews of several drying and wetting approaches were made by Leclerc et al. [1], Ip et al. [2], etc. The approaches to the drying and wetting processes can be broadly classified to two categories: (1) moving mesh approach and (2) fixed mesh approach. The first approach is based on spatially deforming com-

putational meshes. The nodes on the boundary are front-tracking; thus the coordinates of the nodes vary with time. This means that models equipped with this approach include two parts of computations, the hydrodynamic computation and the computation for new mesh generation. This approach is rather expensive because the mesh shall be re-generated with the moving boundary in every time step. Although this moving mesh is proved to be the most precise approach [3,4]; the application can not be extended to a domain with complex boundary, e.g., an estuary with large tidal flats, because the continuous mesh adjustment and re-generation are significant burdens to the model performance.

The fixed mesh technique can be divided into two sub-categories as well. The first sub-category can be referred as the earlier approach suggested by Leendertse [5] in his two-dimensional (2D) model using an alternating direction implicit (ADI) finite difference algorithm. This type of approach "turns off/turns on" the model elements when the water level drops below/above a

---

* Corresponding author. Tel.: +852 2766 6025; fax: +852 2334 6389.
 E-mail address: ceonyx@polyu.edu.hk (O.W.H. Wai).

Nomenclature

$\widetilde{H}$	water depth considering the water volume in capillary
$\widetilde{V}$	water volume including the water in capillary
a	coefficient controlling the decreasing rate of the capillary width
B	Width scale of the capillary
B_s	the minimum width scale of the capillary
f	Coriolis parameter
H	actual water depth $H = \zeta + h$
h	water depth relative to the minimum water level
P_i^*	baroclinic force with Boussinesq assumption
t	time

u, v, ω	velocity components in the x, y, z directions in σ coordinate
U_i	depth averaged velocity components
w	vertical velocity in Cartesian coordinate
x_1, x_2, x_3	spatial coordinates with σ transformation
z_0	elevation of capillary bottom
Z_b	bed elevation, which is equal to $-h$
Δt	time step
$\varepsilon_x, \varepsilon_y, \varepsilon_z$	eddy viscosity coefficients for water
ζ	water level from the minimum water level
τ^b	bottom shear stress
Ω	area of the element
Γ	boundary of the element

threshold water depth, imposes a null value to the velocity components at dry elements, and sets the water level to the bed elevation at the drying process. When it comes to the wetting process the water level at the moving boundary is determined by extrapolating the water level values at the neighboring wet elements (see Fig. 1a). In this type of approach, an artificial slope of the free surface, which generates an extra artificial pressure gradient term, will be formed in the dry area because the water level is arbitrarily fixed at the bed elevation. Leclerc et al. [1] used this approach in a finite element model with the Newton–Raphson solver, and the elements were classified to three types: the dry element, the partially wet (transition) element and the wet element. The treatment of the dry element and wet element was similar to the idea proposed by Leendertse [5]. But for the transition element, in order to eliminate the artificial pressure gradient term, the pressure gradient force and bottom shear stress were dropped out to form a "reduced" momentum equation. Cheng and Smith [6], and Lin and Falconer [7] used a refined algorithm of this type of approach in their 3D layer-integrated models with fixed grids in the vertical direction. In the refined algorithm, there are four steps to check the dry element and three steps for wetting element checking. Although this refined approach is robust, the strict diagnostic tests

are necessary to treat different drying and wetting patterns in the transition elements.

Another approach is based on modifying the hydrodynamic equations to include a cell or an element "size factor" as a function of water depth, e.g., the "marsh porosity method" [2]. In this approach, all the dry and wet areas are computed by assuming that there is water flow in the porous layer below the bed, and the water level can fall below the assigned bed elevation (Fig. 1b). The advantage of this approach is that there are no artificial pressure gradients in the dry elements and there is no need to impose any assumed value on the water elevation and velocity. However, the mass and momentum are not conserved because there are artificial water flows between the dry and wet areas. Some methods have been proposed to reduce this fictitious transport, e.g., Flather and Hubbert [8] and Ip et al. [2] modified the momentum equation by adding a hydraulic conductivity in the porous medium; Heniche et al. [9] increased the bottom shear stress by assuming that Manning coefficient is a function of negative water depth. The main purpose of these methods is to restrain the velocity components, but the mass and conservation can not be satisfied completely unless the velocity components are imposed as zero, which unfortunately will once again lead to the artificial pressure gradient problem.
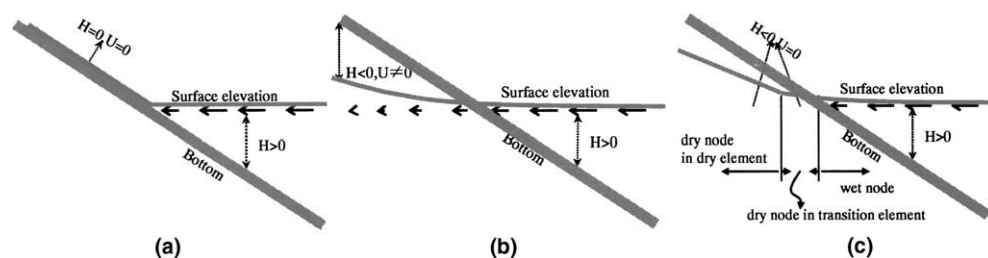

Fig. 1. The hydraulic patterns for approaches: (a) the classical approach (mass conservation); (b) the marsh porosity approach (without artificial slope of the free water surface); (c) the present approach (mass conservation, without artificial slope of the free water surface).

The other problem in this approach is the velocity oscillation when the water depth becomes too shallow. To eliminate this problem, a kinematic approximation, e.g., [2,10,11] was proposed, in which the long-wave equation without the acceleration terms (including the partial time difference and advection terms) was used in shallow estuaries. Erturk et al. [12] shows the negative influence of the kinematic approximation and the relative importance of the lack of local accelerations in a simulation where a standing wave is present. This kind of approximation reduces the model accuracy significantly when the model domain includes areas which are deeper than the tidal flats. McLaughlin et al. [13] shows how local accelerations are added to a 2D model to improve predictions in deeper sections of a well-mixed estuary, while the kinematic approximation is still used on shallow flats.

Most of the approaches mentioned above were developed for 2D models or 3D models with Cartesian/fixed grids in the vertical direction [6,7]. For a 3D model with a bottom following, vertical sigma coordinate system, a highly stable approach for handing the drying and wetting processes is difficult to develop because the grid size may be too small in the vertical direction in the shallow water region.

In this study, a capillary approach is adopted to precisely prescribe the "size factor". The approach was proposed by Tao [14] for a wave model and extended to a 2D shallow water finite difference model by He and Wang [15] and Tao et al. [16]. Li et al. [17,18] found the capillarity effects offered a mechanism to simulate high frequency water table fluctuations at beach faces. The principle of this method is to assume capillaries in the dry areas, and these capillaries connect to the nearby wet areas. In this way the "fictitious" water elevations of all the dry nodes can vary together with the wet nodes and there is no need to "turn off" the dry nodes and "drop out" the artificial pressure gradient term in the transition element. In fact, this approach can be classified in the marsh porosity category as shown in Fig. 1b, nevertheless the capillary approach has a more precise "size factor". Also in the present study, this approach is improved by imposing the velocity components at the dry node as zero, and allowing the water level to drop below the sea bed level with an additional water level diffusion term (Fig. 1c). Through this way, the advantages of the fixed mesh approaches (Fig. 1a and b) can be preserved because both the mass and momentum conservation can be strictly satisfied by rejecting dry areas from the 3D computation, and the artificial slope of the free water surface in transition elements can be avoided. Furthermore, there is not any modification on the momentum equation, and the approach can be implemented easily in any model code.

This improved capillary approach has been implemented in a 3D parallel model developed by Wai et al. [19]. Summary of this model and the details of this new drying and wetting approach are described in this paper.

2. Hydrodynamic model

Since the flow in shallow water can be assumed isothermal and the vertical acceleration is assumed to be small compared to the gravitational acceleration, the hydrostatic assumption is made for the governing equations of the fluid flow. With sigma (σ) topographic following coordinate system used in the vertical direction, the mass conservation and momentum equations are expressed as

$$\frac{\partial \zeta}{\partial t} + \frac{\partial H u_j}{\partial x_j} = 0 \tag{1}$$

$$\frac{\mathrm{d}u_i}{\mathrm{d}t} + f\beta_{ij}u_j + g\frac{\partial \zeta}{\partial x_i} = \frac{\partial}{\partial x_j}\left(\varepsilon_j \frac{\partial u_i}{\partial x_j}\right) \tag{2}$$

where

$$u_j = \{u, v, \omega\},$$
$$\omega = \frac{1}{H}\left[w + (1 - x_3)u_i\frac{\partial h}{\partial x_i} - x_3\left(\frac{\partial \zeta}{\partial t} + u_i\frac{\partial \zeta}{\partial x_i}\right)\right],$$
$$\varepsilon_j = [\varepsilon_x, \varepsilon_y, \varepsilon_z H^{-2}], \quad x_j = [x, y, (z + h)H^{-1}],$$
$$H = h + \zeta, \quad \beta_{ij} = \begin{bmatrix} 0 & -1 & 0 \\ 1 & 0 & 0 \end{bmatrix},$$
$$i = 1, 2, \quad j = 1, 2, 3$$

ζ is the water level from the minimum water level; h is the water depth relative to the minimum water level; t is time; x_1, x_2, x_3 are the spatial coordinates with σ transformation; u, v, ω are the velocity components in the x, y and z directions in the σ coordinate system, respectively; w is the vertical velocity in the Cartesian coordinate system; f is the Coriolis parameter; ε_x, ε_y, ε_z, are the eddy viscosity coefficients for water. The Smagorinsky formula [20] is adopted for estimating the horizontal eddy viscosities ε_x, ε_y; and the vertical eddy viscosity ε_z is calculated according to the 2.5 level turbulent model proposed by Mellor and Yamada [21].

Note that in Eq. (2) the advection term is included in the total time derivative term (the first term in the equation). The discretizaion of this equation is split into three parts, i.e., the advection term, horizontal diffusion term and vertical diffusion term. The numerical details are discussed by Lu and Wai [22]. The first term, advection term, is solved by an Eulerian–Lagrangian method. The second term, horizontal diffusion term, is discretized by an implicit Galerkin finite element method, forming a linear system of sparse symmetric positive-definite coefficient matrix which is solved by the pre-conditioned conjugate-gradient iteration method. The last term, the vertical diffusion term, is discretized by an implicit finite

element method forming a linear system of triangular coefficient matrix which is solved by the double sweep method. The details about the equation system solver and its parallelization can be referred to Wai et al. [19]. In the model, both nine-node quadrilateral and six-node triangular isoparametric elements can be used. The same quadric (second-order) polynomial sharp functions are selected for all the stated variables, such as velocity components, water level, etc.

In this study, the mass conservation equation, Eq. (1), is modified in order to take into account the drying and wetting processes.

unit area = 1). The volume of water taking into account the water inside the capillary, $\widetilde{V}$, is obtained by integrating the capillary area from the bottom to the water surface.

$$\widetilde{V} = \begin{cases} \int_{z_0}^{z_b} (2B - B^2)\,dz + \zeta - z_b, & z_0 < z_b < \zeta \\ \int_{z_0}^{\zeta} (2B - B^2)\,dz, & z_0 < \zeta \leqslant z_b \\ \zeta - z_b, & z_b \leqslant z_0 \end{cases} \quad (5)$$

Submitting Eq. (3) into the above equation and $\widetilde{H}$ can be calculated by $\widetilde{V}$ divided by the unit area.

$$\widetilde{H} \equiv \frac{\widetilde{V}}{1} = \begin{cases} (2B_s - B_s^2)(z_b - z_0) + \frac{2(1-B_s)^2}{\alpha}[1 - e^{a(z_0-z_b)}] - \frac{(1-B_s)^2}{2\alpha}[1 - e^{2a(z_0-z_b)}] + \zeta - z_b, & z_0 < z_b < \zeta \\ (2B_s - B_s^2)(\zeta - z_0) + \frac{2(1-B_s)^2}{\alpha}[e^{a(\zeta-z_b)} - e^{a(z_0-z_b)}] - \frac{(1-B_s)^2}{2\alpha}[e^{2a(\zeta-z_b)} - e^{2a(z_0-z_b)}], & z_0 < \zeta \leqslant z_b \\ \zeta - z_b, & z_b \leqslant z_0 \end{cases} \quad (6)$$

3. Drying and wetting approach

The principle of the capillary method adopted in this study assumes there are huge quantities of capillaries in the bed of dry areas. Fig. 2a and b shows the capillaries in the horizontal and vertical sections. Imposing the possible minimum water level as zero, the bottom (lowest level) of the capillary is z_0 which is set slightly below the minimum water level to guarantee that it is always wet in the capillary, z_b is the bed elevation. Setting the distance between two capillaries to unit length, 1, the width of the capillary, B, is expressed as

$$B = \begin{cases} 1, & z \geqslant z_b \\ B_s + (1 - B_s)e^{\alpha(z-z_b)}, & z_0 < z < z_b \\ 0, & z < z_0 \end{cases} \quad (3)$$

where α is a coefficient that controls the rate of the width reduction; B_s is the minimum width of the capillary.

As mentioned, this approach can be classified in the second fixed mesh category and the vertically integrated mass conservation equation with a size factor, A, can be written as

$$A\frac{\partial \zeta}{\partial t} + \frac{\partial \widetilde{H} U_i}{\partial x_i} = 0 \quad (4)$$

The size factor varies between 0 and 1, it is the area of the capillaries in the horizontal directions, and the value is given by $A = 2B - B^2$; $U_i = \{U, V\}$ is the depth averaged velocity components; $\widetilde{H}$ is the water depth which takes into account the total volume of water above the bed and inside the capillaries, and the value is the volume of water divided by the horizontal area (here, the

Although this approach is similar to the marsh porosity method, the size factor and the water depth are more precisely and smoothly prescribed. In addition, there is no need to modify the momentum equation in this approach. Note the corresponding equation provided by He and Wang [15] and Tao [16] is one-dimensional formula. Here, Eq. (6) is extended to 2D formula.

As mentioned above this approach was used originally in finite difference method and there is a fictitious velocity in the capillary in the dry and partially dry (transition) elements to allow the elevation and other parameters to vary with the neighboring wet elements. Therefore, the shortcomings of this approach are (1) the artificial water transport between the dry and wet areas which may violate the conservation of mass and momentum; (2) in a sensitivity test shown in the later
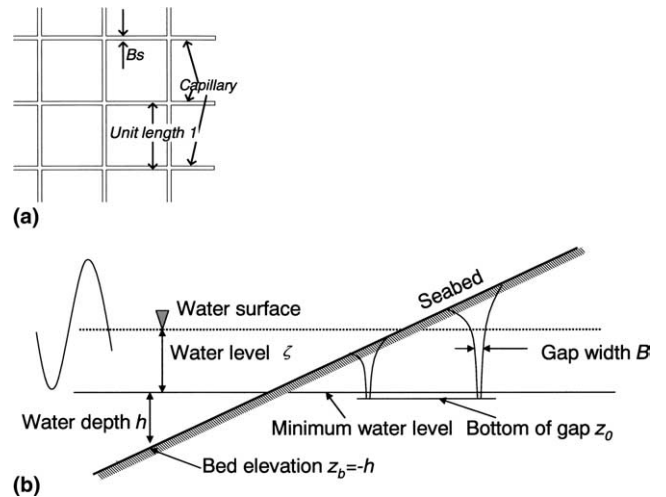

Fig. 2. The capillary pattern in (a) horizontal section (b) vertical section (imposing the minimum water level as zero).

section, the velocity in the dry area oscillates occasionally causing instability problems, and a smaller time step has to be used to overcome the overflow problem.

In this study, the mass and momentum conservation and the model stability are maintained by using the following two strategies: (1) Excluding the dry elements from the 3D momentum computation. This strategy can be implemented by imposing all the velocities of the dry nodes to zero or eliminating the rows of dry nodes from the sparse coefficient matrix. (2) A further modified 2D mass conservation equation is used on both the dry and the wet areas to avoid the artificial slope of the free water surface. This modification is described in detail below.

Based on scale analysis of the momentum equation [23], numerical simulation [24,2] and field observations [25], it is indicated that the pressure gradient and the bottom shear stress are the major physical forces in shallow water processes without stratification. Thus, for shallow and well-mixed water conditions, a simplified vertically integrated momentum equation without the advection and diffusion terms can be expressed as

$$\frac{\partial U_i}{\partial t} + g\frac{\partial \zeta}{\partial x_i} + \frac{\tau_i^{\mathrm{b}}}{H} = 0 \tag{7}$$

Here, τ^{b} is the bottom shear stress. The temporal finite difference representations for Eqs. (4) and (7) are given, respectively as follows:

$$A\frac{\zeta^{n+1} - \zeta^n}{\Delta t} + \frac{\partial \widetilde{H}^n U_i^{n+1}}{\partial x_i} = 0 \tag{8}$$

$$\frac{U_i^{n+1} - U_i^n}{\Delta t} + g\frac{\partial \zeta^{n+1}}{\partial x_i} + \frac{\tau_i^{\mathrm{b}}}{H^n} = 0 \tag{9}$$

in which Δt is the time step. Eliminating U_i^{n+1} by combing Eqs. (8) and (9), the following equation can be obtained:

$$A\frac{\zeta^{n+1} - \zeta^n}{\Delta t} + \frac{\partial(\widetilde{H}^n U_i^n)}{\partial x_i} - \Delta tg\frac{\partial}{\partial x_i}\left(\widetilde{H}^n \frac{\partial \zeta^{n+1}}{\partial x_i}\right)$$
$$- \Delta t\frac{\partial \tau_i^{\mathrm{b}}}{\partial x_i} = 0 \tag{10}$$

In this equation the water level, ζ, may be affected by three terms: (1) the second term in Eq. (10) representing the water current flowing in/out of the nodes; (2) the third term, regarded as the water level diffusion term, which will smooth the water level even when the velocity is zero in the dry nodes; and (3) the last term, the bottom shear stress gradient term, which will vanish in the dry nodes. At a wet node, all the three terms will have influence on the water level. For the dry nodes in a transition element the significance of the first and third terms will reduce because the current becomes smaller compared to the current in the wet elements. But when it comes to the dry nodes in a dry element, only the water level dif-

fusion term will function. Fig. 1c reveals the water level and the flow pattern of this new approach. This modification of the mass equation is first proposed by Lu and Wai [22], they found that it made the computation more efficient when the mass conservation and momentum equations are solved simultaneously. Based on a series of sensitivity tests, it is found that a extremely small value of $\widetilde{H}$ (e.g., $\widetilde{H} < 0.001$ m) at the dry node will restrict the function of the water level diffusion term, leading to an unstable situation caused by the artificial slope of the free water surface in the dry area. In this study, $\widetilde{H}$ is controlled to assure modeling stability as follows:

$$\widetilde{H} = \max(0.05 \text{ m}, \widetilde{H}) \tag{11}$$

This control formula will not affect the computing accuracy as most of the water depth is larger than 0.05 m at the wet area.

In summary, when applying the improved capillary method in the finite element model, the computation is carried out on two equations: the modified vertically integrated mass conservation equation, Eq. (10), and the original 3D momentum equation, Eq. (2). The details about the discretization of Eq. (10) are described in the following section.

4. Implementation of the capillary approach

Eq. (10) makes use of a semi-implicit scheme because the value of $\widetilde{H}$ depends on the node status in the previous time step. Eq. (10) is discretized by a weak Galerkin finite element method. Multiplying the equation with the shape function and applying integration by parts to the divergence terms, the following equation at each element is obtained:

$$\int_\Omega A\frac{\zeta^{n+1} - \zeta^n}{\Delta t}\phi_j \,\mathrm{d}\Omega - \int_\Omega \widetilde{H}^n U_i^n \frac{\partial \phi_j}{\partial x_i} \,\mathrm{d}\Omega$$
$$+ \oint_\Gamma \widetilde{H}^n U_i^n \phi_j \,\mathrm{d}\Gamma + \Delta tg\int_\Omega \widetilde{H}^n \frac{\partial \zeta^{n+1}}{\partial x_i}\frac{\partial \phi_j}{\partial x_j} \,\mathrm{d}\Omega$$
$$- \Delta tg\oint_\Gamma \widetilde{H}^n \frac{\partial \zeta^{n+1}}{\partial n}\phi_j \,\mathrm{d}\Gamma - \Delta t\int_\Omega \frac{\partial \tau_i^{\mathrm{b}}}{\partial x_i}\phi_j \,\mathrm{d}\Omega = 0 \tag{12}$$

Here, the subscript Ω and Γ indicate the area and boundary of the element, respectively. Applying a quadratic six-node triangular element shape function, ϕ_k, to ζ and τ_i^{b}, and ϕ_l to A and $\widetilde{H}$, and then combining Eq. (12) all the elements in the horizontal layer lead to a linear system:

$$\mathbf{G}\zeta^{n+1} = \mathbf{Z} \tag{13}$$

where

$$G_{jk} = J_{jkl}A_l + \Delta t^2 gS_{jkl}\widetilde{H}_l,$$
$$Z_j = J_{jkl}\zeta_k^n A_l + \Delta tE_{jk}\widetilde{H}_k + \Delta t^2 T_{i,jk}\tau_{i,k}^{\mathrm{b}}$$

$$J_{jkl} = \int_\Omega \phi_j \phi_k \phi_l \, \mathrm{d}\Omega, \quad T_{i,jk} = \int_\Omega \frac{\partial \phi_k}{\partial x_i} \phi_j \, \mathrm{d}\Omega,$$

$$E_{jk} = \int_\Omega U_i^n \phi_k \frac{\partial \phi_j}{\partial x_i} \, \mathrm{d}\Omega - \oint_\Gamma U_n^n \phi_k \phi_j \, \mathrm{d}\Gamma$$

$$S_{jkl} = \int_\Omega \phi_l \frac{\partial \phi_k}{\partial x_i} \frac{\partial \phi_j}{\partial x_i} \, \mathrm{d}\Omega - \oint_\Gamma \phi_l \frac{\partial \phi_k}{\partial n} \phi_j \, \mathrm{d}\Gamma,$$

$$j, k, l = 1, \dots, N$$

N is the number of nodes in a horizontal layer. U_n is the velocity normal to the boundary.

The resulting linear equation system, Eq. (13), which includes a sparse non-symmetric positive-definite matrix, **G**, is solved by the pre-conditioned biconjugate-gradient iteration method and the details of this solver are presented by Saad [26].

At the end of the computation of each time step, the status of every node in the entire model domain will be checked to decide whether the node is dry. and the velocity in the dry node will be set to zero. Besides, the water level $\tilde{H}$ of each node will be calculated according to Eqs. (6) and (11). The scanning for flooding nodes, which checks whether a dry node is flooded and determines a water level for the new flooded node, is not necessary because the water level of the dry nodes in a transition element will be achieved automatically by the last three terms of Eq. (10). Therefore, this approach can be easily implemented in a model code.

For the parameters, i.e., a, B_s and Z_0 which describe the capillary properties, Z_0 can be set slightly below the minimum water level and B_s may be a small value such as 0.02 to prevent zero value at the capillary bottom. After a vigorous sensitivity test process, it is found that the optimal value for a is 29 which can minimize the volume of water in the capillary for most of the wetting–drying conditions. Taking the Xiamen Bay application for example, when a is set to 29 the total water depth $\tilde{H}$ calculated by Eq. (6) is larger than the actual water depth H (which does not take into account the volume of water inside the capillary) by 0.1 m at the wetted node in which the bed elevation Z_b is above Z_0 (see Fig. 2). This is an acceptable discrepancy for large-scale estuary simulations.

5. Numerical verification

In order to demonstrate the movement of the water front and to examine the stability of the present capillary approach, a test case and a real application to Xiamen Estuary are described below.

5.1. Basin with variable slope

This test case was used by Leclerc et al. [1] to qualitatively demonstrate the water front movement and to
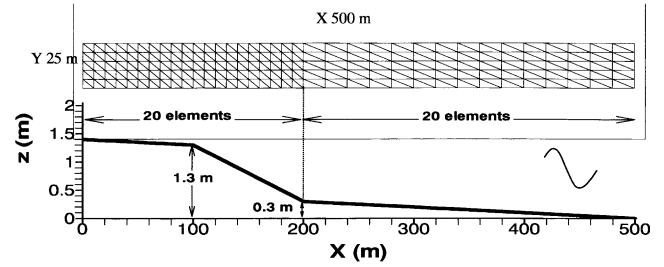

Fig. 3. Basin with variable slope: mesh and geometry.

show the capturing capability of their drying and wetting approach. Heniche et al. [9] adopted the test case to verify a porosity approach as well. Both of approaches produced reasonable results. This test case is taking place in a rectangular basin with a variable slope and the water level is changing with the tidal cycles (see Fig. 3). The basin is 500 m long and 25 m wide, and is discretized with 35 elements in the x direction and 5 elements in the y direction. There are a total of 350 six-node triangular isoparametric elements. The slip condition is set at the close boundary, i.e., at the two side walls and the bottom, with the zero normal velocity. For the open boundary upstream at the right side of the basin, the following time varying tidal elevation is imposed:

$$\zeta = 1.0 + 0.75 \cos(2\pi t / 3600) \tag{14}$$

This means that the tidal cycle has a period of 60 min and an amplitude of 0.75 m. The initial condition for the test case is

$$\zeta = 1.75 \text{ m}; \quad u_i = 0 \tag{15}$$

The time step (Δt) is 9 s, the parameters a, Z_0 and B_s are prescribed as 29, 0.2 m and 0.02, respectively. In order to compare the present approach with the approaches proposed by Leclerc et al. [1] and Heniche et al. [9], the same Manning coefficient and horizontal eddy viscosity coefficient are used which are 0.03 and 5×10^{-2} m²/s, respectively. The Coriolis and baroclinic forces are neglected in the test case.

Since the models of Leclerc et al. [1] and Heniche et al. [9] are 2D models, the drying and wetting prediction capability of the present approach is first demonstrated in a 2D simulation. Fig. 4 shows the hydrodynamic patterns at different time in a tidal cycle including 2D temporal-spatial movement of the water front. During the water level fluctuations, the flow is stagnant at the dry nodes ($U_i = 0$) and the water level changes continuously with the surrounding wet nodes according to the diffusion term in Eq. (10). At $t = 12$ min, there is a significant acceleration of flow near the point $x = 100$ m where and the velocity is about 0.4 m/s, which is the same as the value at the open boundary. This phenomenon has also been observed in the tests of Leclerc et al. [1] and Heniche et al. [9]. The
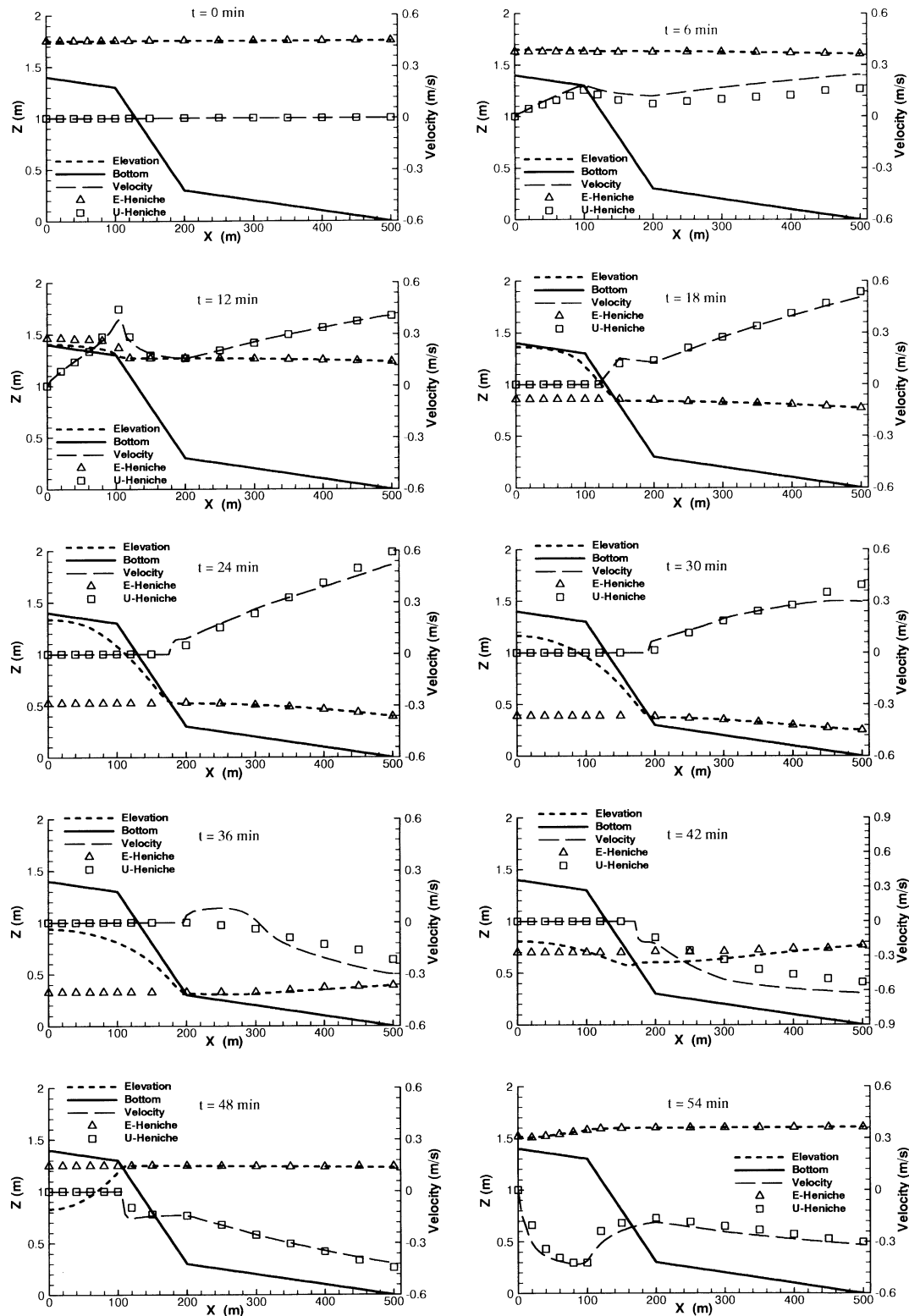
Fig. 4. Results of 2D simulations using the present capillary approach; the delta and square symbols are the elevation and velocity results of Heniche et al. [9], respectively.

results of Heniche et al. [9] are plotted in Fig. 4. Heniche et al. [9] attributed this phenomenon to the spurious oscillations of the water surface level with the same

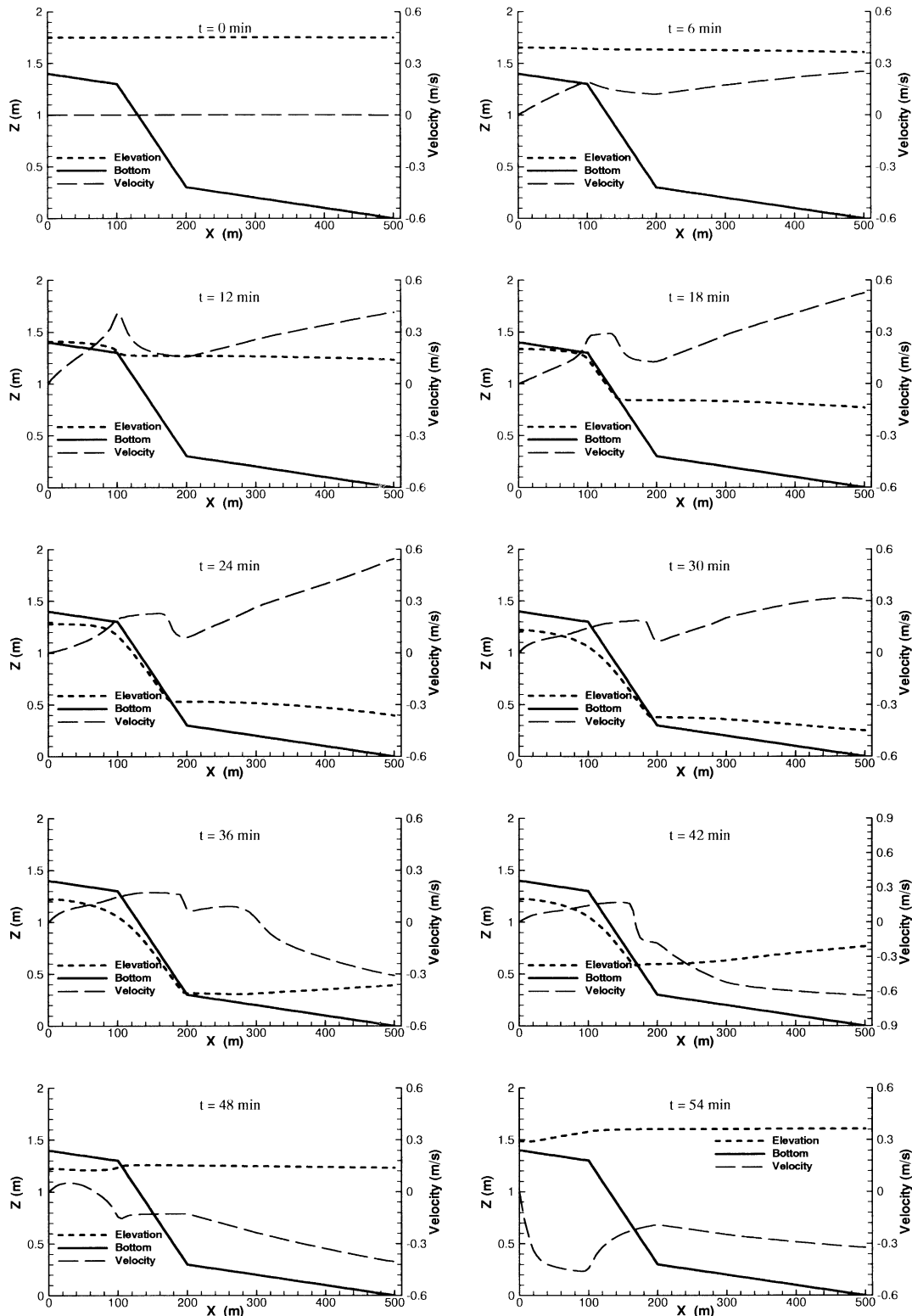order of magnitude as the depth values. Fig. 4 shows that the flow and water level patterns of Heniche et al. [9] and the present capillary approaches are similar.

Fig. 5. Results calculated by the original capillary approach proposed by Tao [16].

The results of Heniche et al. [9] have smoother elevation and velocity pattern near the water front than present capillary approach and Leclerc et al. [1] approach. This is because in the approach of Heniche et al. [9] the advection term and water surface are stabilized by a iso-tropic viscosity and a second-order diffusion operator, respectively, especially in the region 100 m < x < 200 m.

The original capillary method has been tested also with the same parameters. The result (see Fig. 5) reveals that the velocity in the dry area has the same order of
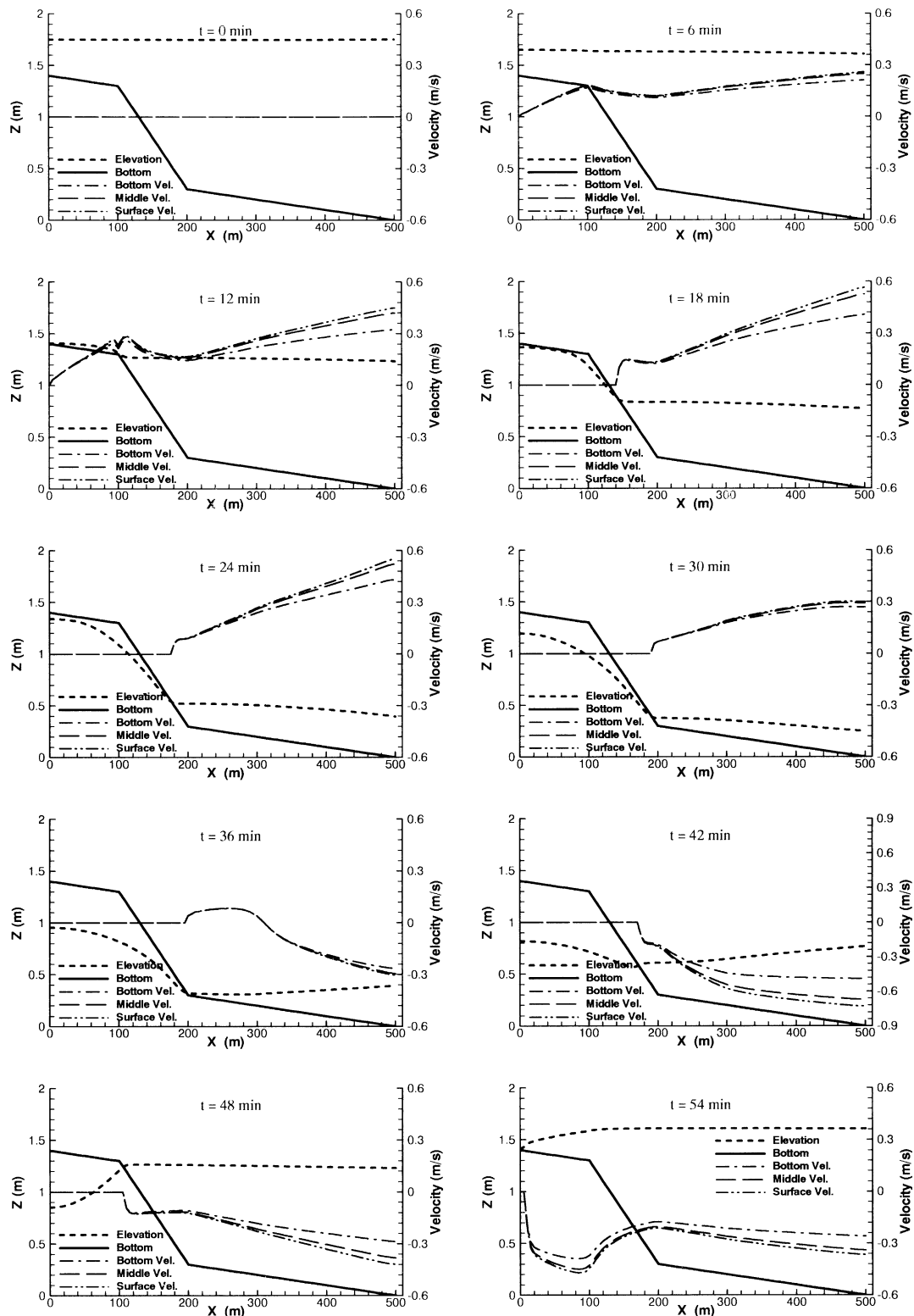
Fig. 6. 3D results calculated by the present capillary approach.

magnitude as in the wet area. This large velocity leads to the artificial water transport between the dry and wet areas, and the oscillating velocity near the water front can decrease the modeling stability.

Fig. 6 shows the computed results of this new approach applied in the 3D finite element model. In this case, the vertical eddy viscosity is fixed at 0.005 m²/s and the time step is 9 s. The water body is divided into

five layers, each horizontal layer has the same element mesh as the above 2D simulation. At $t = 12$ min, there are two velocity maxima around $x = 100$, both of them are less than 0.3 m/s. The water level pattern is generally the same as the one computed in the 2D model simulation with higher velocity at the water surface and lower velocity at water bottom. This implies that the present improved capillary approach can be used in 3D simulations with good modeling stability.

5.2. Application to Xiamen Estuary

Xiamen Estuary (see Fig. 7) is an important harbour in China. In the southeast of the estuary, Xiamen Estuary connects with Taiwan Strait through the two seaward openings separated by Jinmen Island. The tides enter through the two openings to three regions of Xiamen Estuary, i.e., Jiulong River estuary, Western Seas and Eastern Seas. The water depth is relatively shallow in these three regions, and three channels connect these regions with the open sea. The tide of Xiamen Estuary is a typical semi-diurnal tide with a mean tidal range of 3.79 m and a maximum range of 6.24 m. In the west, the Jiulong River discharges into Xiamen Estuary. The total annual runoff volume is 1.5×10^{10} m^3 which only causes insignificant stratification under normal conditions. The tidal current is the major driving force in Xiaman Estuary. Because of the geomorphologic process, large tidal flats appear and the drying and wetting processes are important phenomena in this estuary. The nodal bathymetry in the inner Xiamen Estuary (Western sea and Jiulong Estuary) was interpolated from a navigational chart of 1:5000 scale and for other places, a 1:100,000 navigational chart was used. The tidal flats are indicated by the legend of "Depth < 0" in Fig. 7.

In this application, the model domain is discretized by a total of 4634 six-node triangular elements and 10,444 nodes in each horizontal layer (Fig. 8). The elements are refined at Western Seas because almost all the important cargo terminals are located there and it has large tidal flats. The largest element size is 0.84 km^2 and the minimum is 0.32×10^{-3} km^2. There
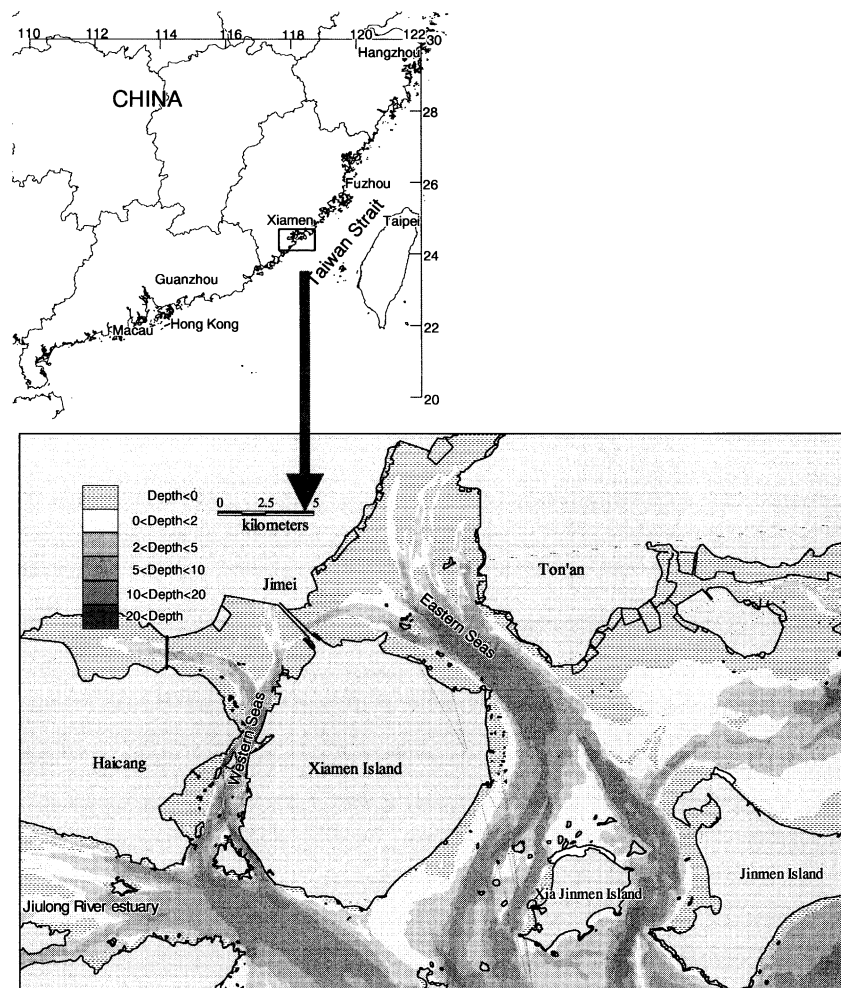

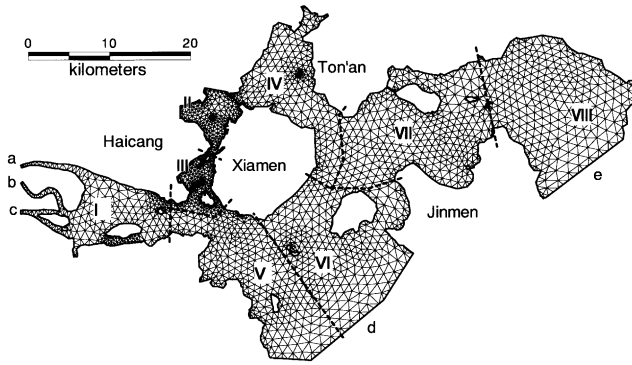Fig. 7. The location and bathymetry of Xiamen Estuary.

Fig. 8. Model mesh for the real life cases: Xiamen Estuary with domain partitioning for parallelization.

are 11 layers in the water column and each layer has the same depth of 1/11th in the sigma coordination system. The model domain is decomposed into eight sub-domains, each of which has about the same number of nodes to achieve a well balanced parallel computation. The Roman numbers in Fig. 8 indicate the number of sub-domains. The horizontal eddy viscosity coefficient is calculated by the Smagorinsky formula [20], and the vertical eddy viscosity coefficient is calculated according to the 2.5-level turbulence model as mentioned previously.

The parallel computer used to run the present simulation is a Beowulf distributed computer system. This system consists of one master and 10 slave processors
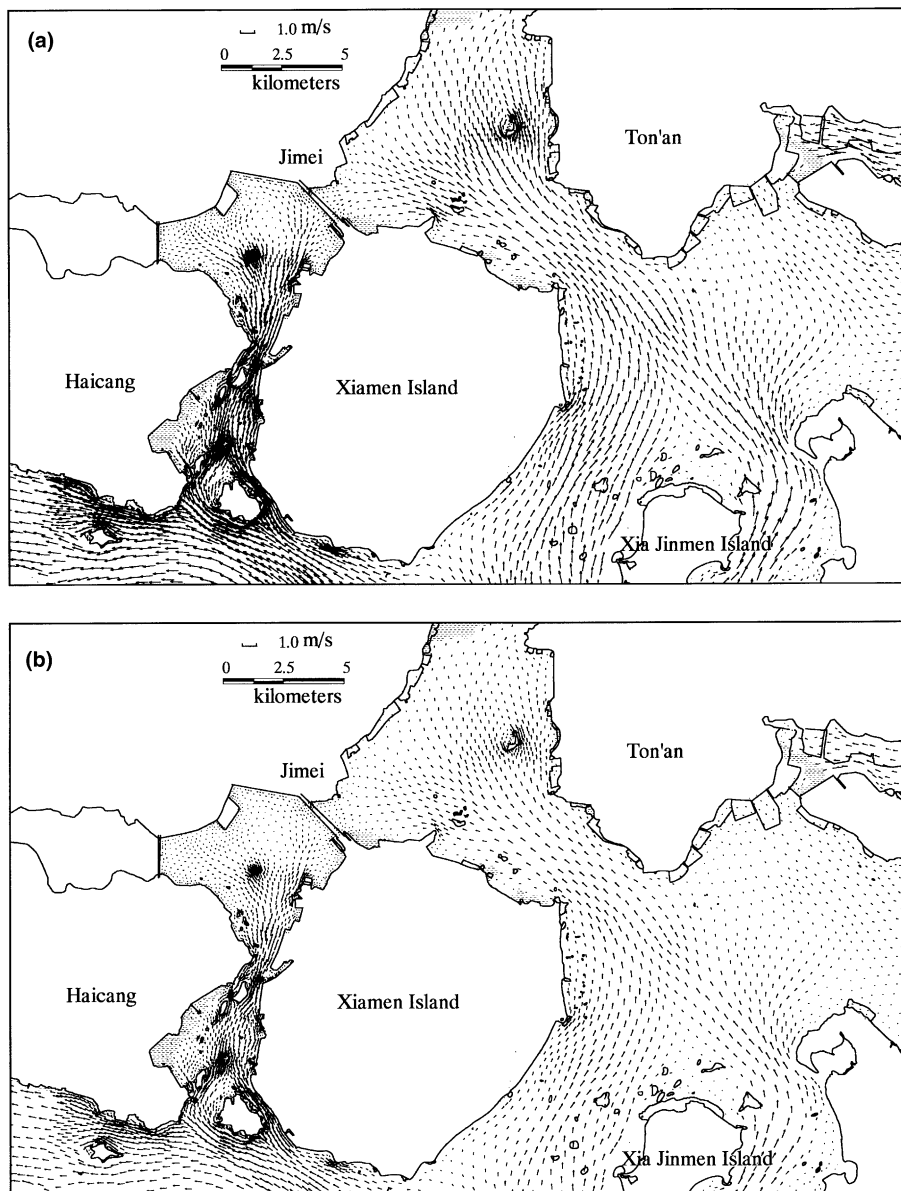

Fig. 9. The computed flow pattern at the sharp flood tide at (a) the surface layer, and (b) bottom layer; the grey blocks indicate the dry areas.

connected with a 100 MB/s switcher. The master processor has a 733 MHz Intel CPU, a 40 GB hard disk and 4 GB memory. Each slave processor has a 733 MHz Intel CPU and 1 GB memory. All the initial information and computed results are stored on the master. The operation system is the Red Hat Linux 6.2, the Message Passing Interface (MPI) is LAM/MPI 6.5.2 provided by University of Notre Dame, and the complier is Lahey FORTRAN 95 Pro 6.0.

For this real application, the capillary width reduction rate a, the capillary bottom Z_0 and the minimum scale width B_s are prescribed as 29, -1 m, and, 0.02, which means a deeper capillary compared with the capillary used in the previous test case. The initial conditions are hydrostatic conditions ($U = 0$, $\zeta = $ constant).

The close boundary is no-slip and impermeable ($U = 0$). There are five open boundaries (Fig. 8), i.e., a, b and c are outlets of Jiulong River, d and e are sea boundaries. All the open boundary conditions are regulated by tidal variations, which are calculated by combining the four major tidal constituents M_2, S_2, N_2 and K_1. The button drag coefficient C_z is estimated by Eq. (16):

$$C_z = \max \left[\frac{k^2}{[\ln(H/N_{z_0})]^2}, 0.0025 \right] \tag{16}$$

where k is the von Karman constant and its value is 0.4; N is the number of layers, Z_0 is the roughness parameter, which is set to 0.01 values.
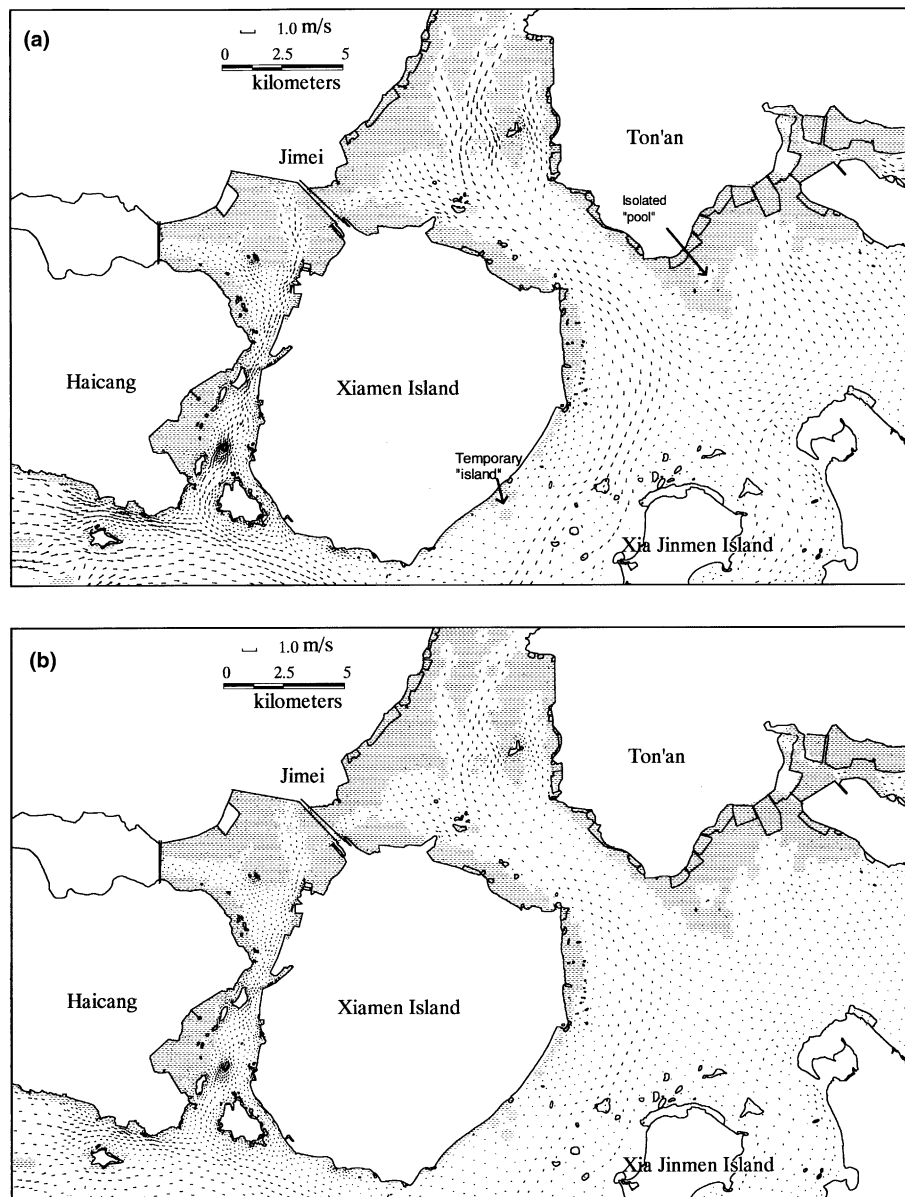

Fig. 10. The computed flow pattern at low slack tide at (a) the surface layer, and (b) bottom layer; the grey block indicates the dry area.

On August 4, 1996, the Third Oceanography Institute of China (Xiamen) conducted a marine survey on several parameters, such as tidal elevation, velocity and sediment concentration. The data at the two tidal stations and the eight velocity stations are used to verify the model results. The averaged relative error at the two tide level stations is less than 4%, and the averaged relative error calculated at all the eight velocity stations, over a 28-h period, is about 16%. The details of the verification of the parallel model can be found in Wai et al. [19].

Fig. 9 shows the computed flow pattern at flood tide. The tidal current is flowing into Eastern Seas and Western Seas, and the surface current is faster than the current near the bottom as expected. During this period there are few dry areas because of the relatively higher water level. But when it comes to the low slack tide, water level drops and large tidal flats begin to show up (Fig. 10). Comparing Figs. 7 and 10, it shows that the tidal flats are reproduced reasonably in Eastern Seas and Western Seas. However, it is also noticed that the tidal flats near Jinmen and east of Ton'an are not simulated properly because of lack of the nodal bathymetry data. In these figures, the tidal flats or dry areas are shown as grey blocks. It is noted that there are a number of isolated "pools" of water appeared in tidal flats, also dried areas (temporary "island") showing up in the wet areas in Fig. 10. These phenomena are caused by the uneven bathymetry in the estuary.

In the simulation, at the ebb tide the water in the "pool" will "penetrate" into the bed (the capillary) and the "pool" area will become dry by the diffusion term in Eq. (10). This area will be wetted again earlier than the surrounding dry areas. This approach can avoid the sharp flooding process when the rising water meets the dried area with lower bed elevation. Since the present approach can reproduce the isolated water "pool" and temporary "island" without stability problems, there is no need to smooth the bottom topography. Furthermore, as seen in this application the stability of the 3D finite element model has not been sacrificed by including the drying and wetting process calculation. The time step used in this application is 200 s, which is the same as the one used by Wai et al. [19] without the consideration of dying and wetting processes.

6. Conclusion

An improved capillary approach is adopted in a 3D sigma finite element model to predict the tidal hydrodynamics in estuaries with large tidal flats. This approach modifies the vertically integrated mass conservation equation and maintains the original form of the momentum equation. Thus, the mass conservation equation can be implemented on both of the dry and wet areas, at the same time the dry areas will be excluded from the 3D momentum computation by imposing the water velocity components to zero. Furthermore, the water elevation in the dry area can drop below the sea bed level to avoid artificial slopes caused by the free water surface in the transition elements. So the advantages of this approach are that (1) the momentum computation does not include the dry areas enabling the 3D model to stably run on the domain of wet area; (2) both the mass and momentum conservation in the wet and dry areas are satisfied; (3) the program can be easily coded because there is no need to check for the flooding nodes.

The test case and the Xiamen Estuary application show that the model incorporated with the capillary approach can accurately simulate the drying and wetting processes in the large tidal flats, and at the same time provide stable 3D hydrodynamic information in the deep regions. The capability to handle the isolated water "pool" in dry areas and temporary "island" in wet areas suggested that tidal flats with discontinuous bathymetry can be modeled by the present approach without any pre-treatment, for example, smoothing the bed elevation before the simulation.

References

[1] Leclerc M, Bellemare JF, Dumas G, Dhatt G. A finite element model of estuarian and river flows with moving boundaries. Adv Water Resour 1990;13(4):158–68.

[2] Ip JTC, Lynch DR, Friedrichs CT. Simulation of estuarine flooding and dewatering with application to Great Bay, New Hampshire. Estuar, Coast Shelf Sci 1998;47:119–41.

[3] Sielecki A, Wurtele MG. The numerical integration of the nonlinear shallow-water equations with sloping boundaries. J Comput Phys 1970;6:219–36.

[4] Lynch DR, Gray WG. Finite element simulation of flow in deforming regions. J Comput Phys 1980;36:135–53.

[5] Leendertse JJ. Water quality simulation model for well mixed estuaries and coastal seas: principles of computation. Rand Corporation, vol. 1, Report No. RM-6230-rc; 1970.

[6] Cheng RT, Smith PE. A survey of three-dimensional numerical estuarine models. Estuarine and coastal modelling conference proceedings. Newport, RI: ASCE; 1989.

[7] Lin B, Falconer RA. Three-dimensional layer-integrated modeling of estuarine flows with flooding and drying. Estuar, Coast Shelf Sci 1997;44:737–51.

[8] Flather RA, Hubbert KP. Tide and surge models for shallow water—Morecambe Bay revisited. In: Davies AM, editor. Modeling marine systems. Boca Raton, FL: CRC Press; 1990.

[9] Heniche M, Secretan Y, Boudeau P, Leclerc M. A two-dimensional finite element drying–wetting shallow water model for rivers and estuaries. Adv Water Res 2000;23:359–72.

[10] LeBlond PH. On tidal propagation in shallow rivers. J Geophys Res 1978;82:4717–21.

[11] Jelesnianski CP, Chen J, Shaffer WA. SLOSH: Sea, lake, and overland surges from hurricanes. NOAA Technical Report NWS, 1992.

[12] Erturk SN, Bilgili A, Swift MR, Brown WS, Celikkol B, Ip JTC, et al. Simulation of the great bay estuarine system: tides with tidal flats wetting and drying. J Geophys Res 2002;107(C5):29.

[13] McLaughlin JM, Bilgili A, Lynch DR. Dynamical simulation of the great bay estuarine system tides with special emphasis on N_2 and S_2 tidal components. Estuar, Coast Shelf Sci 2003;57(1–2): 283–96.

[14] Tao JH. A numerical model of wave running up and breaking on a beach. Acta Oceanol Sinica 1984;6:693–700 [in Chinese].

[15] He SL, Wang LX. Application of the slot method in the computation of two dimensional flow with transient boundary. Shuli Xuebao 1986;12:11–9 [in Chinese].

[16] Tao JH, Li QX, Falconer RA, Lin BL. Modelling and assessment of water quality indicators in a semi-enclosed shallow bay. J Hydraul Res 2001;39(6):611–7.

[17] Li L, Barry DA, Parlange JY, Pattiaratchi CB. Beach water table fluctuations due to wave run-up: capillarity effects. Water Resour Res 1997;33(5):935–45.

[18] Li L, Barry DA, Pattiaratchi CB, Masseelink G. BeachWin: modelling groundwater effects on swash sediment transport and beach profile changes. Environ Model Software 2002;17(3): 313–20.

[19] Wai WHO, Jiang YW, Lu QM. Large scale finite element modeling and parallel computation of sediment transport in coastal areas. In: Lakhan C, editor. Advances in coastal modeling. Netherlands: Elsevier Science; 2003.

[20] Smagorinsky J. General circulation experiments with the primitive equations. Part I: the basic experiment. Month Weather Rev 1963;91:99–164.

[21] Mellor GL, Yamada T. Development of a turbulence closure model for geophysical fluid problems. Rev Geophys Space Phys 1982;20(4):851–75.

[22] Lu Q, Wai O. An efficient operator splitting scheme for three-dimensional hydrodynamic computations. Int J Numer Methods Fluids 1998;26:771–89.

[23] Lu Q. Three-dimensional modeling of hydrodynamics and sediment transport with parallel algorithm. PhD thesis. Hong Kong: Department of Civil and Structural Engineering, The Hong Kong Polytechnic University; 1997.

[24] Friedrichs CT, Madsen OS. Nonlinear diffusion of the tidal signal in frictionally dominated embayments. J Geophys Res 1992;97: 5637–50.

[25] Swift MR, Brown WS. Distribution of bottom stress and tidal energy dissipation in a well-mixed estuary. Estuar, Coast Shelf Sci 1983;17:297–317.

[26] Saad Y. Iterative methods for sparse linear systems. PWS Publishing Company; 1996.